The Cryosphere Discuss., 7, 1029–1074, 2013
www.the-cryosphere-discuss.net/7/1029/2013/
doi:10.5194/tcd-7-1029-2013

The Cryosphere Discussions
Open Access

Data assimilation and prognostic whole ice-sheet modelling with the variationally derived, higher-order, open source, and fully parallel ice sheet model VarGlaS

D. J. Brinkerhoff and J. V. Johnson

University of Montana, Missoula, MT, USA

Received: 12 February 2013 – Accepted: 14 Februar 2013 – Published: 8 March 2013

Correspondence to: D. J. Brinkerhoff (douglas.brinkerhoff@umontana.edu)

Published by Copernicus Publications on behalf of the European Geosciences Union.

Abstract

We introduce a novel, higher order, finite element ice sheet model called VarGlaS (Variational Glacier Simulator). Contrary to standard procedure in ice sheet modelling, VarGlaS formulates ice sheet motion as the minimization of an energy functional, conferring advantages such as a consistent platform for making numerical approximations, a coherent relationship between motion and heat generation, and implicit boundary treatment. VarGlaS also solves the equations of enthalpy rather than temperature, avoiding the solution of a contact problem. Rather than include a lengthy model spin-up procedure, VarGlaS possesses an automated framework for model inversion. These capabilities are brought to bear on several benchmark problems in ice sheet modelling, as well as a 500 yr simulation of the Greenland ice sheet at high resolution. VarGlaS performs well in benchmarking experiments, and given a constant climate, predicts an overall mass evolution of the Greenland ice sheet that matches well with observational data.

1 Introduction

Models have become an important tool in the study of glacier and ice sheet physics, with applications to the prediction of cryosphere/climate interactions, sea level rise, and fundamental questions of ice dynamics. In recent years, while conceptual and theoretical advances in the development of ice sheet models have been made, computational constraints limited practical ice sheet models to low-order asymptotic approximations of ice physics. Early models (and some modern ones) relied upon the shallow ice approximation, sacrificing accuracy in regions of complex flow for efficiency at large scales. Models including higher order physics were also used, but the increased computational demand made operating at high resolutions infeasible. Additionally, many models were based on finite difference schemes, which made variable resolutions over different regions in the computational domain difficult. Recent increases in computing

TCD
7, 1029–1074, 2013

power and the availability of parallel libraries, in tandem with the finite element method and unstructured meshes have made possible the use of higher order physical approximations coupled with the high resolution necessary to resolve fine scale features of glacier flow. The ice sheet modelling community has been quick to take advantage of these advances, for example in Larour et al. (2012); Seddik et al. (2012); Leng et al. (2012), and Bueler and Brown (2009), among others. In this work, we present a new thermomechanically coupled, prognostic ice sheet model called VarGlaS (Variational Glacier Simulator). As stated above, there are already a few examples of so-called "next generation" ice sheet models in existence, but this model differs in implementation strategy in several critical regards. Namely, these are the use a of a variational principle in the model formulation, the solution of an enthalpy equation, the use of a kinematic boundary condition, and the use of automatic differentiation for data assimilation.

VarGlaS treats the solution to the momentum balance (Stokes' equations) as the minimization of an energy functional. The existence of a variational principle for non-linear Stokes' flow was shown by Bird (1960). When applied to ice sheets, the method consists minimizing the dissipation of gravitational potential energy by viscous and frictional heat generation. This approach has been suggested by Schoof (2006); Dukowicz (2012), and Bassis (2010). This type of treatment stands in contrast to the heretofore standard treatment of the velocity field, which is to explicitly account for the balance of viscous stresses and forcing by gravity, as is done in most other ice sheet models (e.g. Larour et al., 2012; Seddik et al., 2012; Leng et al., 2012; Bueler and Brown, 2009; Rutt et al., 2009). Viewing the problem as a variational minimization problem confers a number of advantages. The most important advantage is that the momentum balance is uniformly derived from a single scalar conservation statement. When approximations to the physics are made, they are made to the scalar quantity, and these changes are automatically propagated through the rest of the model. This is particularly useful in case where tools for automatic differentiation exist, as is the case in this model. The procedure of generating the code for a new approximation to the Stokes' equations is as simple as making a change to the variational principle. This makes extension of

TCD
7, 1029–1074, 2013

the model to different asymptotic approximations straightforward. Other potential advantages are that the variational principle is coordinate independent, streamlining the transition to a curvilinear or geographic coordinate system. Boundary conditions are also implicitly defined within the variational principle, meaning that the often complex process of imposing boundary conditions is simplified. The use of a variational principle also confers several computational advantages. For example, the operators derived from the variational principle are guaranteed to be at least symmetric and semi-definite. Also, these operators are already in the appropriate form for use with the finite element method, requiring no further manipulation.

Treatment of the energy balance by VarGlaS also differs from standard methods. Typically, temperature is the variable of interest in the energy balance (Larour et al., 2012; Seddik et al., 2012; Greve and Hutter, 1995; Rutt et al., 2009; Pattyn, 2003). Computing the temperature field is a contact problem where the temperature must be constrained to remain below the phase boundary. Different methods have been employed to enforce this constraint, such as treating temperate and cold ice as two separate fluids Greve and Hutter (1995), and manipulating heat sources and sinks such that heat sources are applied to the temperature equation when below the melting point and to calculate a melt rate when the ice is at the pressure melting point Rutt et al. (2009). To avoid inconsistency and heuristics, we eschew the temperature formulation in favor of an enthalpy treatment that tracks total internal energy density rather than sensible heat. This eliminates the need for special numerical treatment of the cold-temperate transition surface, at the expense of introducing a nonlinearity in energy diffusion (Aschwanden et al., 2012). While enthalpy is more straightforward computationally, the temperature field is still necessary for the computation of ice rheology and for interpretation of model results. Temperature can be recovered from enthalpy in a straightforward way through a bijection between enthalpy, temperature, and water content.

VarGlaS is equipped with a kinematic boundary condition that allows for the evolution of ice geometry. Many models calculate change in surface elevation as the flux divergence of the vertically averaged horizontal velocity field (Larour et al., 2012; Rutt et al.,

TCD
7, 1029–1074, 2013

2009; Bueler and Brown, 2009). We treat it as the advection of the ice surface by the surface velocity field, as is done in Seddik et al. (2012) and Leng et al. (2012). The two forms are equivalent, and both are numerically unstable. VarGlaS, similar to other modern finite element models, uses streamline upwind Petrov–Galerkin finite elements to stabilize the free surface problem (Larour et al., 2012; Seddik et al., 2012). Additionally, transitions between glaciated and ice-free regions of the model domain produce numerical instabilities which need to be addressed with methods beyond upwinding in order to maintain higher order accuracy. To this end, VarGlaS also introduces a discontinuity capturing scheme to maintain stability in the presence of large gradients. VarGlaS uses a unique and fully explicit total variation diminishing Runge–Kutta scheme for time discretization. This method guarantees that no new spurious extrema are generated by the time stepping scheme, and provides second order in time accuracy without necessitating a complex and expensive coupling between the momentum balance and time evolution.

For both diagnostic and prognostic modelling, it is important to constrain the model to match observed values of state variables as closely as possible. To this end, VarGlaS possesses tools for data assimilation. With automatic differentiation in hand, calculating the adjoint state of a model and the gradient of a given objective function with respect to arbitrary parameters under the constraint that a forward model be satisfied is simple and automated. We use this capability in two complementary ways. First, we have been able to invert for sliding velocity (or basal traction) to best match surface velocities, a classic problem in glacier modelling (MacAyeal, 1993; Goldberg and Sergienko, 2011; Larour et al., 2005; Gudmundsson and Raymond, 2008; Morlighem et al., 2010; Brinkerhoff et al., 2011). In contrast to many implementations of data assimilation in ice sheet modelling (MacAyeal, 1993; Morlighem et al., 2010), VarGlaS uses an unsimplified adjoint (Goldberg and Sergienko, 2011; Brinkerhoff et al., 2011). We can also minimize the total imbalance in mass continuity with respect to basal topography (e.g. Morlighem et al., 2011), although this procedure is presented in a separate paper (Johnson et al., 2013). These methods are important for long term simulations, as the

TCD
7, 1029–1074, 2013

former reproduces a plausible velocity that is of leading order importance in calculating surface rates of change, while the latter helps to eliminate strong transients resulting from estimates of basal topography that are incoherent relative to the ice physics and observed data.

The paper is structured as follows. Section 2.1 discusses the continuum mechanical formulation of the model physics. Section 2.2 deals with the numerical implementation of the model physics, and the difficulties arising from their discretization. Section 3 involves the application of the model to a few numerical experiments including well known benchmarks involving idealized geometry, as well as the entire Greenland ice sheet. Finally, in Sect. 4 we discuss some of the things which our model does well, and what aspects require further refinement.

2 Model

VarGlaS can solve for the three dimensional ice sheet velocity, temperature, and geometry through time. All three of these variables are strongly coupled. We first present the continuum formulation of ice sheet physics, followed the numerical treatment for each.

2.1 Physics

2.1.1 Momentum balance

Our development of a variational principle for the momentum balance largely follows Dukowicz (2012). The variational principle for a power law rheology with linear basal

TCD
7, 1029–1074, 2013

sliding under the constraints of incompressibility and bed impenetrability is:

$$\mathcal{A}[\boldsymbol{u},P] = \int_{\Omega} \Bigg[\underbrace{\frac{2n}{n+1}\eta\left(\dot{\epsilon}^2\right)\dot{\epsilon}^2}_{\text{Viscous Dissipation}} + \underbrace{\rho \boldsymbol{g}\cdot\boldsymbol{u}}_{\text{Potential}} - \underbrace{P\nabla\cdot\boldsymbol{u}}_{\text{Incomp.}} \Bigg] \mathrm{d}\Omega + \int_{\Gamma_B} \Bigg[\underbrace{\frac{\beta^2}{2}h^r \boldsymbol{u}\cdot\boldsymbol{u}}_{\text{Friction}} + \underbrace{P\boldsymbol{u}\cdot\boldsymbol{n}}_{\text{Impen.}} \Bigg] \mathrm{d}\Gamma, \quad (1)$$

where $\boldsymbol{u}$ is the ice velocity and $\dot{\epsilon}$ the rate of strain tensor, P is the pressure, $\eta(\dot{\epsilon}^2)$ the strain rate dependent ice viscosity, $\boldsymbol{g}$ the gravitational vector, β^2 the basal sliding coefficient, h the ice thickness, r a factor determining the relationship between basal traction and thickness, and $\boldsymbol{n}$ is the outward normal vector. The expression is minimized over the ice domain Ω with boundaries Γ. Each of the additive terms in Eq. (1) has a specific meaning. Terms integrated from left to right over Ω are viscous dissipation, gravitational potential energy, and the incompressibility constraint, respectively. Terms under the boundary integral are frictional heat dissipation and the impenetrability constraint. The constitutive relationship for ice given by Glen (1955) gives a viscosity of

$$\eta(\dot{\epsilon}^2) = b(T,\omega)[\dot{\epsilon}^2]^{\frac{1-n}{2n}}, \quad (2)$$

where $\dot{\epsilon}^2$ is defined to be the square of the second invariant of the strain rate tensor, and $b(T,\omega)$ is a temperature and water content dependent rate factor

$$b(T,\omega) = \left[E\,a(T,\omega)e^{-\frac{Q(T)}{RT^*}}\right]^{\frac{-1}{n}}. \quad (3)$$

Here, E is an enhancement factor, $a(T,\omega)$, $Q(T)$, and R are parameters, and T^* is temperature corrected for pressure melting point dependence. The traditional momentum

TCD
7, 1029–1074, 2013

balance form of the Stokes' equations can be recovered (in weak form) by taking the variation of Eq. (1). This is the functional that VarGlaS minimizes in order to solve the Stokes' problem.

The Stokes' functional is a relatively complete statement of ice physics (the only assumptions being negligible inertial terms), but it includes four degrees of freedom per computational node (three velocity components and pressure) and is a saddle point problem due to the presence of the Lagrange multiplier pressure terms. A considerable simplification can be made to the Stokes' functional by expressing vertical velocities in terms of horizontal ones through the incompressibility and bed impenetrability constraints, that is

$$w(\boldsymbol{u}_{\|}) = -\int_{B}^{z} \nabla_{\|} \cdot \boldsymbol{u}_{\|} \, \mathrm{d}z' \tag{4}$$

with boundary condition

$$w_b = \boldsymbol{u}_{\|b} \cdot \nabla_{\|} B. \tag{5}$$

Substitution of these expressions into $\mathcal{A}$ yields an unconstrained and positive definite integro-differential functional which is equivalent to Eq. (1). However, the integral terms that result from the vertical integration of the mass conservation equation are undesirable. Standard methods for the numerical solution of PDEs are not equipped to handle integral terms of this type, so we seek a simplification that eliminates them. In order to derive the functional associated with the so-called "first order" equations of ice sheet motion (Blatter, 1995; Pattyn, 2003), two assumptions must be made. First, bed slopes are small, which is also equivalent to assuming cryostatic pressure. Second, horizontal gradients of vertical velocity are small compared to other components of the strain rate tensor. This eliminates vertical velocity terms. After these assumptions and some

TCD
7, 1029–1074, 2013

manipulation, the first order functional is

$$\mathcal{A}_1[\boldsymbol{u}_\parallel] = \int_\Omega \left[\underbrace{\frac{2n}{n+1}\eta\left(\dot{\epsilon}_1^2\right)\dot{\epsilon}_1^2}_{\text{Viscous Dissipation}} + \underbrace{\rho g \boldsymbol{u}_\parallel \cdot \nabla_\parallel S}_{\text{Potential}} \right] \mathrm{d}\Omega$$
$$+ \int_{\Gamma_s} \left[\underbrace{\frac{\beta^2}{2} h^r \boldsymbol{u}_\parallel \cdot \boldsymbol{u}_\parallel}_{\text{Friction}} \right] \mathrm{d}\Gamma, \tag{6}$$

where $\boldsymbol{u}_\parallel$ is the velocity vector in the horizontal directions, S is the elevation of the ice surface, and $\dot{\epsilon}_1^2$ is the first order strain rate tensor given by Pattyn (2003) and Dukowicz (2012). Since the first order equations are only associated with horizontal velocity components, this formulation yields a significant computational savings, as well as desirable numerical properties such as guaranteed positive definiteness. Vertical velocity is recovered from Eqs. (4) and (5).

2.1.2 Enthalpy

VarGlaS uses an enthalpy formulation of the energy balance (Aschwanden et al., 2012). Enthalpy methods track total internal energy, rather than sensible heat, which corresponds bijectively to temperature for ice below the pressure melting point, and to water content for ice at the pressure melting point. The enthalpy equation is a typical advection-diffusion equation with a non-linear diffusivity

$$\rho(\partial_t + \boldsymbol{u}\cdot\nabla)H = \rho\nabla\cdot\kappa(H)\nabla H + Q, \tag{7}$$

where H is enthalpy, ρ is ice density, and Q is strain heat generated by viscous dissipation, given by the dissipative term in the momentum balance functional. κ is an

TCD
7, 1029–1074, 2013

enthalpy dependent diffusivity given by

$$\kappa(H) = \begin{cases} \dfrac{k}{\rho C_p} & \text{if cold} \\ \dfrac{\nu}{\rho} & \text{if temperate,} \end{cases} \tag{8}$$

where k is the thermal conductivity of cold ice and C_p is heat capacity. ν is the diffusivity of enthalpy in temperate ice, and can also be thought of as a parameterization of the sub-grid scale intraglacial flow of liquid water. It is not clear what the value of ν should be. Both Hutter (1982) and Aschwanden and Blatter (2009) have suggested that it be a function of both water content and gravity, but intra-glacial liquid modelling is beyond the scope of this work and we usually set this value to either zero, or some constant much less than $\frac{k}{C_p}$. This implies that heat does not move diffusively within temperate ice, and that any heat generation immediately goes towards melting. The definitions for cold and temperate ice are as follows:

$$\begin{cases} \text{cold} & (H - h_i(P)) < 0 \\ \text{temperate} & (H - h_i(P)) \geq 0 \end{cases} \tag{9}$$

where h_i is the pressure melting point expressed in enthalpy,

$$h_i(P) = -L + C_\mathrm{w}(T_0 - \gamma P), \tag{10}$$

and C_w is the heat capacity of liquid water, γ is the dependence of the melting point on temperature, T_0 is the triple point of water, and L is the latent heat of fusion for water.

At the ice surface, we specify a Dirichlet boundary condition corresponding to surface temperature. At the basal boundary we apply the Neumann boundary condition

$$\kappa(H)\nabla H \cdot \boldsymbol{n} = q_\mathrm{g} + q_\mathrm{f} - M_\mathrm{b}\rho L, \tag{11}$$

TCD
7, 1029–1074, 2013

where q_g is geothermal heat flux, assumed known, q_f is frictional heat generated by basal sliding, and M_b is the basal melt rate. Frictional heat is given by the frictional term in the momentum balance functional. Note that in temperate ice, where $\kappa(H)$ is zero (no diffusion), this relation defines the basal melt rate. In cold ice, a value must be specified for the basal melt rate (which can be negative). We usually take this to be zero.

Enthalpy is uniquely related to temperature and liquid water in the following way:

$$T(H,P) = \begin{cases} C_p^{-1}(H - h_i(P)) + T_m(p) & \text{if cold} \\ T_m & \text{if temperate} \end{cases}$$

$$\omega(H,P) = \begin{cases} 0 & \text{if cold} \\ \dfrac{H - h_i(P)}{L} & \text{if temperate,} \end{cases} \tag{12}$$

where ω is fractional water content and h_i and T_m are the pressure melting points expressed in enthalpy and temperature, respectively.

2.1.3 Dynamic boundaries

The ice sheet geometry evolves over time according to the kinematic boundary condition

$$(\partial_t + \boldsymbol{u}_\parallel \cdot \nabla_\parallel)S = w + \dot{a}, \tag{13}$$

where $\dot{a}$ is the accumulation rate.

2.1.4 Marine outlet treatment

VarGlaS currently treats the grounding line in the simplest way possible, which is to keep its location fixed. At this point, ice can not become ungrounded. For transient runs, the geometry of calving fronts is fixed, so that mass loss due to calving is effectively

TCD
7, 1029–1074, 2013

proportional to the velocity at the calving front. At the scale of outlet glaciers, this is a limitation and is a major priority in ongoing development.

2.2 Numerical methods

The above section presented the continuum equations governing ice dynamics. In the following sections, we discuss how these equations are discretized in order to be made computationally tractable.

2.2.1 Finite element discretization using FEniCS

VarGlaS is built upon the finite element package FEniCS (Logg et al., 2012). FEniCS is a powerful development environment for performing finite element modelling, including strong support for symbolic automatic differentiation, native parallel support and parallel interface with linear algebra solvers such as PETSc (Balay et al., 2012) and Trillinos (Heroux et al., 2005), and automatic code generation and compilation for compiled performance from an interpreted language interface. The Python scripting environment makes the generation and linking of new code straightforward. We find that this interface provides a level of extensibility that makes VarGlaS promising for distributed development and rapid prototyping of models for additional components of the cryosphere.

FEniCS has a large library of finite elements available. We use only one, the continuous, linear Lagrange finite element, defined over an unstructured triangular mesh. This choice of element is unstable for advection dominated equations, such as the kinematic boundary condition and the enthalpy equation (in most cases), as well as for Stokes' equations due to the pressure term. We cover stabilization procedures in the following sections.

The velocity field and enthalpy equations are both non-linear. These are each solved by using a relaxed Newton's method (e.g. Deuflhard, 2004) with a Jacobian calculated

TCD
7, 1029–1074, 2013

by automatic differentiation

$$\mathbf{J}[U^n]\Delta U = -F[U^n] \tag{14}$$

$$U^{n+1} = U^n + R\Delta U \tag{15}$$

where U^n is the solution vector at the nth iteration, ΔU is a solution update, $\mathbf{J}$ is the Jacobian matrix, and F is the system of non-linear equations. R is a relaxation parameter that arbitrarily shortens the step size in order to improve numerical stability. The amount of damping required is specific to the problem, but we find that a relaxation parameter between 0.7 and 1.0 is typically sufficient to achieve convergence. We specify both a relative and absolute tolerance as convergence criteria for Newton's method. The solution is considered converged if the L_∞ norm of ΔU is less than $1 \times 10^{-6}\,\mathrm{m\,a^{-1}}$ or the L_∞ norm of $\frac{\Delta U}{U^n}$ is less than 1×10^{-3}.

In order to resolve the coupling between enthalpy and velocity, we use a fixed point iteration. Each of these non-linear equations are solved independently, and the result is iteratively used as input in calculating the other variable. Convergence is assumed when both the velocity and temperature updates are less than $1 \times 10^{-6}\,\mathrm{m\,a^{-1}}$ and $1 \times 10^{-6}\,\mathrm{K}$, respectively.

2.2.2 Mesh refinement

The model domain is discretized using a tetrahedral mesh which is unstructured in the horizontal dimensions, and structured in the vertical. In order to equidistribute discretization error, we use the classic anisotropic error metric

$$\boldsymbol{e}(c) \propto \max_{i \in E} \boldsymbol{x}_i^T \boldsymbol{M} \boldsymbol{x}_i, \tag{16}$$

where $\boldsymbol{e}(c)$ is a cellwise error estimate, E a given mesh cell, x_i an edge in E and $\boldsymbol{M}$ a metric tensor, in this case defined by

$$\boldsymbol{M} = \boldsymbol{V}^T |\boldsymbol{\Lambda}| \boldsymbol{V}. \tag{17}$$

TCD
7, 1029–1074, 2013

$\boldsymbol{V}$ and $\boldsymbol{\Lambda}$ are the respective eigenvectors and eigenvalues of the Hessian matrix of the field over which error is to equidistributed (Habashi et al., 2000). For all the meshes presented forthwith, we use the Hessian of an observed velocity norm (either observed or modelled) in calculating error metrics. A discrete approximation for each component of the Hessian matrix is obtained iteratively for each level of mesh refinement by solving the variational problem

$$\int_\Omega \mathrm{Hess}_{ij}\phi \,\mathrm{d}\Omega = -\int_\Omega \frac{\partial U}{\partial x_i}\frac{\partial \phi}{\partial x_j}\,\mathrm{d}\Omega + \int_\Gamma \frac{\partial U}{\partial x_i}\phi n_{x_i}\,\mathrm{d}\Gamma, \tag{18}$$

where Hess_{ij} are the components of the Hessian and U is the surface speed. With error estimates in hand, we isotropically refine all cells that are above a specified proportion of the average error. In order to account for the directional nature of the velocity field, we incorporate anisotropy by using Gauss–Seidl iterations to approximately solve an elasticity problem, with computed edge errors as "spring constants". This mixed isotropic–anisotropic technique yields high quality and efficient meshes with both the structural simplicity of isotropic refinement, as well as the better error to mesh size ratio of anisotropic techniques. An example of a mesh created with this method is shown in Fig. 1.

2.2.3 Data assimilation and regularization

Many physical quantities of leading order relevance to glacier and ice sheet flow are either practically impossible to collect, or are point measurements which cannot generally be extrapolated to a broader spatial context. Examples of the former include historic variables such as a detailed record of surface temperature or ice impurity content at deposition. Examples of the latter include basal water pressure, basal temperature, enhancement factors, and geothermal heat flux. A particularly important parameter which must usually be estimated is the coefficient of basal traction, which relates basal shear stress to sliding velocity. In many cases, sliding makes up nearly all of a glacier's

TCD
7, 1029–1074, 2013

surface velocity (e.g. Weis et al., 1999). Thus, any model that wishes to reproduce plausible velocity and thermal structures must parameterize traction. The availability of widespread surface velocity data, and the conceptually simple relationship between surface and bed velocities have made the inversion of surface velocities for basal traction a popular choice for performing this parameterization (MacAyeal, 1993; Goldberg and Sergienko, 2011; Larour et al., 2005; Gudmundsson and Raymond, 2008; Morlighem et al., 2010; Brinkerhoff et al., 2011).

We have implemented basal traction inversion in VarGlaS using a partial differential equation constrained optimization procedure. In the following, we illustrate the method using surface velocity in the cost functional, and basal traction as the control variable, but the procedure is analogous for any choice of objective function of control variable. The fundamental concept behind this method is to define a scalar objective function, to calculate its gradient, and to use standard minimization techniques to find the minimum. We use a general form for the definition of the cost functional $\mathcal{J}'$. Examples include a linear cost functional:

$$\mathcal{J}'[\boldsymbol{u}] = \int_{\Gamma_s} \|\boldsymbol{u} - \boldsymbol{u}_{\text{obs}}\| \, \mathrm{d}\Gamma \tag{19}$$

or a logarithmic one

$$\mathcal{J}'[\boldsymbol{u}] = \int_{\Gamma_s} \left[\log \frac{\|\boldsymbol{u}\|}{\|\boldsymbol{u}_{\text{obs}}\|} \right]^2 \mathrm{d}\Gamma. \tag{20}$$

We require the velocity field obtained by this functional satisfy the equations of motion by imposing the momentum equations via a Lagrange multiplier:

$$\mathcal{J}[\boldsymbol{u}, \beta^2] = \mathcal{J}' + \delta \mathcal{A}[\boldsymbol{u}, \beta^2; \lambda], \tag{21}$$

where δ implies the first variation operator, and $\mathcal{A}$ is one of the energy functionals defined in Sect. 2.1.1. λ is a Lagrange multiplier used to enforce the forward model as

TCD
7, 1029–1074, 2013

a constraint. Taking the variation of $\mathcal{J}$ with respect to $\boldsymbol{u}$, β^2, and λ yields, respectively, a forward model, an adjoint model, and an expression for the gradient of the objective function with respect to β^2 which is expressed in terms of $\boldsymbol{u}$ and λ. Note that no simplifying assumptions about the nature of the forward model are made. In particular, when possible we use the full adjoint, calculated via automatic differentiation, rather than making the assumption that the viscosity not depend on $\boldsymbol{u}$ as is done in many inversion procedures (e.g. Goldberg and Sergienko, 2011; Larour et al., 2012). In the case where strong mismatches between the modelled and surface velocity exist, stability of the inversion numerics necessitates fixing the viscosity, and using an incomplete adjoint, as in Goldberg and Sergienko (2011), but only for the first few iterations.

In order to impose a minimum bound on the smoothness of the solution, we add a Tikhonov regularization term, which penalizes wiggles in the control variable. This regularization is of the form

$$\mathcal{T} = \alpha \int_{\Gamma_B} \|\nabla\beta^2 \cdot \nabla\beta^2\| \, \mathrm{d}\Gamma, \tag{22}$$

where α is a positive weighting tensor. This value is different for different objective functions and different model domains. Note that applying Tikhonov regularization on the gradient in this way is equivalent to applying an anisotropic diffusion operator to the control variable.

With a means of efficiently computing the objective function and its gradient with respect to the control variable in hand, we can use any number of optimization algorithm to minimize $\mathcal{J}$. We use the quasi-newton algorithm L_BFGS_B (Nocedal and Wright, 2000). We used a parallel implementation of the L_BFGS_B algorithm derived from that appearing in the dolfin-adjoint library (Farrell et al., 2013). Termination criterion for the optimization routine is essentially heuristic, with the optimization procedure terminating upon the objective function reaching a valley. The definition of a reliable convergence criterion is a subject of ongoing research, with the methods of Habermann et al. (2012) particularly promising.

TCD
7, 1029–1074, 2013

2.2.4 Time evolution

We use two different algorithms for the discretization of time.

For the enthalpy equation, we use a semi-implicit Crank–Nicholson time stepping scheme, with ALE treatment of the convective velocities in order to compensate for the moving mesh (Donea et al., 2005). This semi-implicit method is acceptable because of the relatively minor nonlinear coupling between enthalpy and the velocity field; linearization is achieved by calculating the non-linear dependence with the values of the previous time step. Crank–Nicholson provides second order accuracy in time, provided that the Courant–Friederich–Lewy criterion

$$\Delta t \max\left(\kappa \frac{1}{\boldsymbol{h}\cdot\boldsymbol{h}}, \boldsymbol{u}\cdot\frac{1}{\boldsymbol{h}}\right) \leq C \tag{23}$$

is satisfied, where $\boldsymbol{h}$ is the vector of cell dimensions in each direction and C is a constant, usually taken to be $\frac{1}{2}$. Note that this condition can be restrictive in some outlet glaciers, where the combination of 1 km scale spatial resolution, and $> 1\,\mathrm{km\,a^{-1}}$ scale velocities require time steps on the order of a month.

For the free surface equation, the nonlinear coupling between velocity and surface elevation is stronger, so linearization is not a desirable option, and solving the full nonlinear problem implicitly is inefficient. We instead choose to use a fully explicit total variation diminishing Runge–Kutta (TVD-RK) type scheme of second or third order (Gottlieb and Shu, 1998). The total variation diminishing property implies that no spurious oscillations should be created as a result of the time discretization. This must be coupled with a non-oscillatory spatial discretization (such as streamline upwinding) in order to maintain a stable solution. The TVD property is important in suppressing spurious oscillations near sharp margins (such as those characterizing glacial termini). Being a Runge–Kutta method, we must solve the momentum balance once for each order of accuracy, but we find that the added stability and accuracy of using a higher order explicit method makes this increase in computational overhead worthwhile.

TCD
7, 1029–1074, 2013

2.2.5 Stabilization

Both the enthalpy and free surface equations are hyperbolic and the standard centered Galerkin fnite element method gives rise to spurious oscillations. In order to provide stabilization, we apply streamline upwind Petrov–Galerkin (SUPG) methods (Brooks and Hughes, 1982). For the enthalpy equation, this consists of adding an additional diffusion term of the form

$$\rho \nabla \cdot K \nabla H, \tag{24}$$

where K is a tensor valued diffusivity defined by

$$K_{ij} = \frac{\alpha h}{2} \frac{u_i u_j}{\|\boldsymbol{u}\|}, \tag{25}$$

α is taken equal to unity, and h is a cell size metric. Alternatively, we can view this stabilization as using skewed finite element test functions

$$\hat{\phi} = \phi + \frac{\alpha h}{2} \frac{\boldsymbol{u}}{\|\boldsymbol{u}\|} \cdot \nabla \phi \tag{26}$$

to weight the advective portion of the governing equation. Since the time derivative is implicitly defined, there is no need to apply upwind weighting to the time derivative or source terms, and because linear elements are used, applying this weighting to the diffusive component would necessitate second derivatives of test functions, which are always zero for linear elements.

For the free surface equation, a similar procedure is used, where modified Galerkin test functions

$$\hat{\phi} = \phi + \frac{h}{2} \frac{\boldsymbol{u}_\parallel}{\|\boldsymbol{u}_\parallel\|} \cdot \nabla_\parallel \phi \tag{27}$$

TCD
7, 1029–1074, 2013

are used to discretize the equations. Note that in this case, due to the explicit time stepping scheme, the augmented weighting function is applied consistently to the entire residual, including the time derivative. In addition to streamline upwinding, we apply a shock-capturing artificial viscosity in order to smooth the sharp discontinuities that occur at the ice boundaries, where the model domain switches from ice to ice-free regimes. This additional term is given by

$$D_{\text{shock}} = \nabla \cdot C \nabla S \tag{28}$$

where C is the nonlinear residual-dependent scalar

$$C = \frac{h}{2\|\boldsymbol{u}\|}[\nabla_{\|} S \cdot \nabla_{\|} S]^{-1} \mathcal{R}^2. \tag{29}$$

Here, $\mathcal{R}$ is the residual of the original free surface equation.

For the Stokes' equations to remain stable, it is necessary to either satisfy or circumvent the Ladyzhenskaya–Babuska–Brezzi (LBB) condition. The typical way of doing this is to use a mixed second order in velocity, first order in pressure finite element (the Taylor–Hood element). While VarGlaS has the capacity to use this formulation, we find that the additional degrees of freedom introduced by the higher order elements leads to an unacceptable loss of computational performance. Instead, we circumvent this condition by using a Galerkin-least squares (GLS) formulation of the Stokes' functional

$$\mathcal{A}'[\boldsymbol{u}, P] = \mathcal{A} - \int_{\Omega} \tau_{\text{gls}} (\nabla P - \rho \boldsymbol{g}) \cdot (\nabla P - \rho \boldsymbol{g}) \, \mathrm{d}\Omega, \tag{30}$$

where τ_{gls} is a stabilization parameter (Baiocchi et al., 1993). For a linear Stokes' problem, the usual value for τ_{gls} is

$$\tau_{\text{gls}} = \frac{h^2}{12\eta}. \tag{31}$$

TCD
7, 1029–1074, 2013

Since τ_{gls} is a function of the ice viscosity, τ_{gls} should rightly be nonlinear. However, we have found through experimentation that ignoring the strain rate dependence of the viscous term yields acceptable results and much better numerical stability. Thus we use

$$\tau_{\text{gls}} = \frac{h^2}{12\bar{\eta}}. \tag{32}$$

where $\bar{\eta}$ is some linear estimate of η. We have found $\bar{\eta} = 10^3 \times b(T)$ to yield an appropriate blend of fidelity to the governing equations and stabilization. Note that this has the effect of adding a diffusive term over pressure to the conservation of mass equation.

2.2.6 Parallelism

VarGlaS has been developed to take full advantage of the innate parallel capabilities of PETSc (Balay et al., 2012) and FEniCS (Logg et al., 2012), on which it is built. All computationally intensive components of the model are compatible with parallel usage, such as the nonlinear solvers, time stepping, and optimization. VarGlaS exhibits good scaling between 1 and 16 cores, the largest cluster to which the authors have access. Parallel efficiency for a non-linear solution of the first order equations over all of Greenland for over a million degrees of freedom is shown in Fig. 2.

3 Numerical experiments

In order to assess the correctness and efficiency of model, we apply it to a number of well known ice sheet modelling benchmark experiments, before turning it towards a large scale data assimilation and prognostic time stepping simulation for the whole Greenland ice sheet.

TCD
7, 1029–1074, 2013

3.1 ISMIP-HOM

The Ice Sheet Model Intercomparison Project – Higher Order Model (ISMIP-HOM) benchmarks are a widely used test of higher order model capabilities (Pattyn et al., 2008). In order to verify our model performance, we run ISMIP-HOM tests A, C, and F using both the first order and Stokes' equations for the momentum balance.

ISMIP-HOM A simulates steady ice flow with no basal slip over a sinusoidally varying bed with periodic boundary conditions. Figure 3 shows the simulated surface velocity for all length scales outlined in the benchmark.

ISMIP-HOM C simulates steady ice flow with sinusoidally varying basal traction over a flat bed with periodic boundary conditions. Figure 4 shows the simulated surface velocity for all length scales outlined in the benchmark. This experiment specifies that r equal zero in the sliding law.

After running the ISMIP-HOM C experiment forward, we have in hand the velocity field predicted by the model for a given basal traction. We used this as an opportunity to test the inverse capabilities of the model, and to invert for a known basal traction. Starting from an initial guess of a uniform basal traction of $1000\,\mathrm{Pa\,a\,m^{-1}}$, we allow the inverse model to predict the basal traction field that produces the velocity field of the forward model (which we know to be a sinusoid). In this case we used a length scale of $L = 80\,\mathrm{km}$. Figure 5 shows both the rate of convergence, as well as the "observed" and modelled basal tractions and surface velocities along the $L/4$ transect of the ISMIP-HOM model domain.

ISMIP-HOM F simulates unsteady ice flow over a Gaussian bump with periodic boundary conditions under slip and non-slip conditions, and evaluates the surface geometry and velocity as they relax to steady state. Figure 6 shows the simulated surface velocities and elevations for the slip and non-slip cases.

TCD
7, 1029–1074, 2013

3.2 EISMINT II

The European Ice Sheet Model INTercomparison II (EISMINT II) benchmarks are an older set of benchmarks than ISMIP-HOM, and were designed for use with models employing the shallow ice approximation (Payne et al., 2000). While ISMIP-HOM generally tests the accuracy of the momentum balance scheme over varying length scales, the EISMINT experiments are more focused towards assessing the time dependent mass and energy balances. EISMINT II stresses the dynamic evolution of the system and provides a test for the long term stability of our time stepping scheme. We know of no other higher order model operating on an unstructured grid that has demonstrated a capacity to run forward on such time scales.

In EISMINT II A, a radially symmetric surface mass balance and temperature field are imposed on an initially ice free, flat bed. The model geometry and temperature field are allowed to evolve for 200 ka. At the end of this period the total energy and mass were changing by less than $1 \times 10^{-4}\,\%\,a^{-1}$, implying near steady state conditions. Figure 7 shows the resulting thickness and basal temperature fields. Thickness and basal temperature at the center point of the ice sheet were 3647 m and 255.4 K respectively. These are important metrics for intercomparison performance, and lie near the benchmark means of 3688 m and 255.605 K.

EISMINT II F is identical to experiment A, except that imposed surface temperatures are 15° colder throughout the model domain. The results of this experiment are similar to those of experiment A, albeit with a thicker ice sheet, and a slightly different basal temperature profile. The resulting thickness and basal temperature fields are given by Fig. 7 An interesting difference between the resulting temperature field here, and that documented in the EISMINT II paper, is that VarGlaS does not predict the breakdown in radial symmetry that occurred in all of the finite difference models of the intercomparison. We suspect that this is due to VarGlaS using an unstructured grid, which alleviates some of symptoms of grid dependency seen in the original experiment.

TCD
7, 1029–1074, 2013

3.3 Greenland

We applied VarGlaS to a large scale problem in glaciology, namely the transient simulation of the Greenland ice sheet. The strategy in so doing was to initialize the model using measured present day geometry, apply data assimilation tools to obtain an initial estimate of the basal traction field, and then allow Greenland's geometry, velocity, and temperature to evolve over 500 yr. We performed all simulations of Greenland using the first order approximation for the momentum balance (see Eq. 6).

3.3.1 Data

We relied on the SeaRISE model setup for input data (SeaRISE, 2012). Bedrock and surface geometry were from Bamber et al. (2001) with updated basal topography in the Jakobshavn region from CReSIS, surface temperatures from Fausto et al. (2009), basal heat fluxes from Shapiro and Ritzwoller (2004), and surface mass balances from Ettema et al. (2009). We used InSAR derived 2007–2008 average surface velocities from Joughin et al. (2010) for a surface velocity target. The Joughin dataset is incomplete. The gaps were filled with balance velocities, with gradients between the two reduced by systematically exploring the uncertainties in the accumulation rate.

3.3.2 A mesh for Greenland

The boundary of Greenland was digitized using the 1 m contour of the Bamber et al. (2001) thickness data. We created an initial two-dimensional (map plane) mesh by imposing a 2 km element size at the margins, grading to a variable but much coarser resolution at the center of the ice sheet. This ensured that the mesh captured the complexity of the boundary , while maintaining appropriate coarseness in the interior. We refined the mesh using the techniques of Sect. 2.2.2. We extruded this footprint over ten vertical layers. Greenland, when more highly resolved in the vertical dimension, demonstrates convergence problems during the Newton's method solution process.

TCD
7, 1029–1074, 2013

Although we cannot definitively say why higher vertical resolutions do not converge, we suspect that it is a result of very low aspect ratio elements producing poor conditioning or round-off error in the Jacobian matrix. This is a significant limitation, and attempts to overcome it are ongoing.

3.3.3 Data assimilation

We calculated a basal traction field using the techniques of Sect. 2.2.3. We begin by calculating steady state velocity and enthalpy fields for an arbitrary basal traction (with an initial guess of $4\,\mathrm{Pa\,a\,m^{-2}}$), with r equal to unity (which implies that basal traction is linearly scaled by thickness; this effectively eliminates the dependence of sliding speed on normal force, and eliminates the covariance between β^2 and H). With this initial state in hand, we ran the BFGS algorithm, using a fixed viscosity (and an incomplete adjoint) for the first ten iterations, before switching to a full adjoint. The temperature field was also recomputed every fifty evaluations of the objective function in order to maintain thermal equilibrium. After the first ten iterations, the velocity field was visually indistinguishable from that of the data, and the convergence between temperature and velocity fields became a fixed point iteration on the enthalpy field. The BFGS algorithm was allowed to run for 200 evaluations of the objective function. Convergence of the algorithm is shown in Fig. 8. The observed and modelled velocities, along with basal traction and temperature fields are shown in Fig. 9. To illustrate some of the fine scale detail of both the mesh and the data assimilation result, Fig. 10 shows a closeup of Helheim glacier in eastern Greenland. The velocity field matches the observed closely. For outlet glaciers like Helheim, we see that surface velocity can be explained by a basal traction composed of both low traction streaming features, and sticky pinning points that slow flow. Basal temperature is also related to basal traction, where fast sliding is associated with a melted bed.

TCD
7, 1029–1074, 2013

3.3.4 Prognostic run

After performing the data assimilation procedure outlined above, we allowed the ice sheet to evolve through time for 500 yr under the C1 (constant climate) SeaRISE experiment. The present day surface elevation of Greenland is not in exact alignment with model physics, and large transient signals propagate through the system at the beginning of the run. We monitored the size of these transients as the L_∞ norm of the $\partial_t S$ field, given by Fig. 12. Note the exponential decay rate; this gives some estimate of how much relaxation a model requires in order to eliminate transients. Results from Pritchard et al. (2009) show that the average $\partial_t S$ of the GrIS is $-0.84\,\mathrm{m\,a^{-1}}$. An ice sheet model should have relaxed at least to this level before any conclusions should be drawn from additional forcing being applied to it. We also monitored the mass of the entire ice sheet through time. After the initial transient period of ice increase, we found an annual average total ice decrease of $1 \times 10^{-3}\,\%\,\mathrm{a^{-1}}$, which is in order-of-magnitude agreement with the GRACE derived ice loss of approximately $6 \times 10^{-3}\,\%\,\mathrm{a^{-1}}$ (Baur et al., 2009). Otherwise, the qualitative pattern of velocity, geometry, and temperature change relatively little over the 500 yr run.

4 Discussion

VarGlaS performs well in a number of standard benchmarking experiments and can also simulate the evolution of the GrIS using higher order physics and thermomechanical coupling, as well as an advanced treatment of time evolution.

For the diagnostic and isothermal ISMIP-HOM benchmark experiments, both VarglaS' first-order and Stokes' solvers perform well with respect to existing benchmark results, with our first-order solver generally predicting values close the the Stokes' mean, and our Stokes' solver generally predicting velocities slightly slower than those reported by the benchmark. Our data assimilation procedure is able to effectively reproduce these simple imposed basal traction fields through model inversion. Both first-order

TCD
7, 1029–1074, 2013

and Stokes' solvers performed well on the prognostic ISMIP-HOM F, yielding velocity and surface elevation fields that are in better agreement with a pseudo-analytical perturbation analysis solution from Gudmundsson (2003) than most participating models. Results for the EISMINT II experiments are similar, with model results comparing favorably to mean values from the original publication. Also, thickness and temperature fields compare well with the results of Pattyn (2003) and Saito et al. (2003) who also applied higher-order models to these experiments. Note that this is the first time that the EISMINT II experiments have been performed with a higher-order finite element model using an unstructured mesh.

VarGlaS' behaviour over the entire Greenland ice sheet echoes what has been determined by various investigators in the past, which is that after the relaxation of a strong transient signal derived from the incompatibility of flawed basal topography, surface velocities, and surface mass balance data, the ice sheet seems to be losing mass on the order of $1 \times 10^{-3}\,\%\,a^{-1}$. Performing simulations of this temporal length and at this spatial resolution has only been made possible by a combination of advances in ice sheet modelling technology, namely variable spatial resolution, data assimilation, and parallelism.

We used an adjoint model derived from automatic differentiation to invert the model at continental scale, yielding plausible velocity fields. Inversion was a critical step for a few reasons; insofar as the measured velocity and surface elevation fields are correct and the geometry of the ice sheet is self-consistent, the inversion procedure minimizes transient signals, and allows the model to reach a self-consistent state more quickly than would be otherwise possible with a less-sophisticated starting procedure. This reasoning extends to the calculation of a starting enthalpy field, which would be of a much lower quality without incorporating the very significant heat source due to friction at the bed.

We employed an anisotropically refined, variable resolution mesh in order to minimize superfluous degrees of freedom in slowly varying regions of the ice sheet while maintaining detailed solutions in regions of large velocity gradients. Although variable

TCD
7, 1029–1074, 2013

resolution modelling is not impossible with finite differences (Colella et al., 2000), it is applicable to finite elements in a straightforward way.

Parallelism was another critical component in modelling the whole Greenland ice sheet. The number of degrees of freedom is simply too large for one processor to handle in a reasonable amount of time. We found that we retained better than 50 % parallel efficiency for nearly one million degrees of freedom and sixteen processors, using an iterative solver. This corresponds to a speedup of around a factor of ten. With the increasing availability of large computers with many processors, the benefit of incorporating parallelism into model design is clear.

VarGlaS currently does not possess a detailed treatment of marine terminal processes, namely grounding line migration dynamics and a prognostic calving law. Each of these presents its own computational and theoretical challenges. It is well known that grounding line dynamics operate at a scale that is typically sub-grid relative to the whole ice sheet field equations (Nowicki, 2007; Favier et al., 2012). In most cases, accurate positioning of the grounding line probably does not greatly affect the evolution of an ice sheet at a continental scale. Nevertheless, scenarios such as the potential collapse of the West Antarctic ice sheet due to a fundamentally unstable bed geometry provide a strong motivation for getting these physics right. VarGlaS is in a good position to incorporate a detailed treatment of grounding line dynamics. The detailed spatial resolution necessary for capturing the physics can be managed by the existing mesh refinement code. Additionally, VarGlaS also possesses robust free surface stabilization that will certainly be necessary for performing simulations of grounding line migration on complex, real world topography. A prognostic calving would also be necessary to accurately simulate grounding line dynamics. VarGlaS currently does not have the capacity to move the lateral bounds of its computational domain. Leaving this boundary fixed and imposing a known-thickness boundary is equivalent to making the assumption of a constant and balanced calving rate. This is likely valid for short and medium term continental scale model runs. This treatment is insufficient for short term,

TCD
7, 1029–1074, 2013

regional scale experiments such as modelling the response of inland glaciers to ice shelf collapse.

Data assimilation is an essential part of correctly modelling ice surface velocities. Without using inverse methods to estimate the value of the basal traction field, the observed pattern of surface velocities is not well reproduced, and the present day ice configuration is not (and should not be) captured. Additionally, without relying on inverse methods, long and computationally expensive spin-up procedures are required, which are not feasible from a processing standpoint, even with the efficient structure of VarGlaS and other modern ice sheet models. Simultaneously, we must recognize the limitations of inverting for the basal traction field. The inversion is ill-posed and often lacks a physically motivated stopping point for optimization algorithms. Even with the inclusion of a regularization term, there generally exist multiple solutions for the basal traction field that produce plausible surface velocity results (although many qualitative features must exist in all solutions). This lack of uniqueness makes drawing conclusions about basal conditions at specific points from inverted models tenuous. Also, the inversion procedure does not allow for time dependency of the basal traction field. Basal traction is believed to be fundamentally linked to subglacial water routing and pressure. Under changing climate scenarios, delivery of water to the bed may change dramatically, and this could fundamentally alter basal traction. Similarly, changes in ice sheet geometry are expected to change the pattern of basal traction through changes in ice overburden pressure as well as surface elevation forced water input. For a non-trivial portion of the ice sheet, basal traction is a zero order control on all model physics. Long term prognostic simulations involving major changes in climate or ice sheet geometry must include a mechanism for estimating changes in basal traction.

With the major increases in efficiency gained from parallelism and anisotropic mesh refinement, it is tempting to model on increasingly detailed meshes, simply due the philosophy that this will give us more detailed and thus more meaningful results. In an ideal scenario, in which the data from which we draw our surface elevations, bed elevations, surface velocities, and surface mass balances are effectively error-free and

TCD
7, 1029–1074, 2013

at spatial resolutions much finer than the grids on which we model. This may have been the case in the past, when the errors derived from using the shallow ice approximation were larger than those inherent in data, and low spatial resolution grids could average from a number of data points falling within a given pixel. It is certainly not the case now. It is simple to generate meshes with a horizontal resolution of near an ice thickness, but it is not simple to determine how to accurately interpolate from 5 km thickness data down to this resolution. Nevertheless, in some heavily studied regions of the GrIS, data at thickness-scale horizontal resolution exists (e.g. Jakobshavn, Russell-Isunnguata Sermia), and this should be incorporated when possible. For the future, we intend to incorporate error metrics over all of VarGlaS's input data into our mesh generation procedure, in order to avoid obtaining spurious results and using unnecessary computational resources as a result of over-resolving in regions where the data are not at a commensurate level of detail.

5 Conclusions

In this paper, we have introduced a novel next-generation ice sheet model called VarGlaS. VarGlaS is built upon the Finite Element package FEniCS, and borrows heavily on FEniCS' innate capabilities, with such features as automatic differentiation of the adjoint state, an interface to a variety of efficient solvers, and demonstrably scalable parallelism. VarGlaS eschews the common stress balance formulation of ice flow physics in favor of formulation as the problem of minimizing a scalar variational principle representing the conversion of gravitational potential energy into heat under the constraint of incompressibility. We use an enthalpy formulation for the energy balance equations, exchanging the temperature equation's contact problem for additional nonlinearity. VarGlaS treats conservation of mass using the kinematic boundary condition.

We applied VarGlaS to the ISMIP-HOM benchmarks for higher order models, as well as several of the EISMINT II experiments. VarGlaS performed well in all of these benchmarks, proving that it correctly solves the field equations. Additionally, we applied

TCD
7, 1029–1074, 2013

VarGlaS's data assimilation to one of the benchmark experiments, showing that it can recover a simple basal traction field from an observed velocity field.

We then turned model to diagnostic and prognostic simulation of the Greenland ice sheet. We began by solving for basal traction using interferometrically derived surface velocities. Using this basal traction field, and other data from the SeaRISE dataset, we solved for the geometry, temperature, and velocity of Greenland 500 yr into the future. We found that after a brief period of relaxing transient signals, the model predicts a $1 \times 10^{-3}\,\%\,a^{-1}$ decrease in total mass over the 500 yr period.

6 Code repository

A developmental version of VarGlaS including many of the experiments discussed above is available at http://code.launchpad.net/um-feism.

Acknowledgements. Brinkerhoff was supported by NASA grant *NASA EPSCoR NNX11AM12A*. Johnson was supported by NASA grant *NASA EPSCoR NNX11AM12A* and National Science Foundation grant *NSF 0504628*.

References

Aschwanden, A. and Blatter, H.: Mathematical modeling and numerical simulation of polythermal glaciers, J. Geophys. Res., 114, F01027, doi:10.1029/2008JF001028, 2009. 1038

Aschwanden, A., Bueler, E., Khroulev, C., and Blatter, H.: An enthalpy formulation for glaciers and ice sheets, J. Glaciol., 58, 441–457, doi:10.3189/2012JoG11J088, 2012. 1032, 1037

Baiocchi, C., Brezzi, F., and Franca, L. P.: Virtual bubbles and Galerkin-least-squares type methods (Ga. L. S.), Comput. Method. Appl. M., 105, 125–141, doi:10.1016/0045-7825(93)90119-I, 1993. 1047

Balay, S., Brown, J., Buschelman, K., Gropp, W. D., Kaushik, D., Knepley, M. G., McInnes, L. C., Smith, B. F., and Zhang, H.: PETSc Web page, http://www.mcs.anl.gov/petsc, 2012. 1040, 1048

TCD
7, 1029–1074, 2013

Bamber, J. L., Layberry, R. L., and Gogineni, S. P.: A new ice thickness and bed data set for the Greenland ice sheet 1. Measurement, data reduction, and errors, J. Geophys. Res., 106, 33773–33780, doi:10.1029/2001JD900054, 2001. 1051

Bassis, J. N.: Hamilton's principle applied to ice sheet dynamics: new approximations for the large-scale flow of ice sheets, J. Glacial., 56, 497–513, 2010. 1031

Baur, O., Kuhn, M., and Featherstone, W.: GRACE-derived ice-mass variations over Greenland by accounting for leakage effects, J. Geophys. Res.-Sol. Ea., 114, B06407, doi:10.1029/2008JB006239, 2009. 1053

Bird, R. B.: New variational principle for incompressible non newtonian flow, Phys. Fluids, 3, 539, doi:10.1063/1.1706087, 1960. 1031

Blatter, H.: Velocity and stress fields in grounded glaciers: a simple algorithm for including deviatoric stress gradients, J. Glaciol., 41, 331–344, 1995. 1036

Brinkerhoff, D. J., Meierbachtol, T. W., Johnson, J. V., and Harper, J. T.: Sensitivity of the frozen/melted basal boundary to perturbations of basal traction and geothermal heat flux: isunnguata Sermia, western Greenland, Ann. Glaciol., 52, 43–50, doi:10.3189/172756411799096330, 2011. 1033, 1043

Brooks, A. N. and Hughes, T. J.: Streamline upwind/Petrov–Galerkin formulations for convection dominated flows with particular emphasis on the incompressible Navier–Stokes equations, Comput. Method. Appl. M., 32, 199–259, doi:10.1016/0045-7825(82)90071-8, 1982. 1046

Bueler, E. and Brown, J.: Shallow shelf approximation as a "sliding law" in a thermodynamically coupled ice sheet model, J. Geophys. Res., 114, F03008, doi:10.1029/2008JF001179, 2009. 1031, 1033

Colella, P., Graves, D. T., Keen, N., Ligocki, T. J., Martin, D. F., McCorquodale, P., Modiano, D., Schwartz, P., Sternberg, T., and Straalen, B. V.: Chombo Software Package for AMR Applications – Design Document, unpublished, 2000. 1055

Deuflhard, P.: Newton Methods for Nonlinear Problems: Affine Invariance and Adaptive Algorithms, vol. 35 of Springer Series in Computational Mathematics, Springer, Berlin, 2004. 1040

Donea, J., Huerta, A., Ponthot, J., and Rodriguez-Ferran, A.: Arbitrary Lagrangian–Eulerian methods, in: Encyclopedia of Computational Mechanics, 1, 2005. 1045

Dukowicz, J. K.: Reformulating the full-Stokes ice sheet model for a more efficient computational solution, The Cryosphere, 6, 21–34, doi:10.5194/tc-6-21-2012, 2012. 1031, 1034, 1037

TCD
7, 1029–1074, 2013

Ettema, J., van den Broeke, M. R., van Meijgaard, E., van de Berg, W. J., Bamber, J. L., Box, J. E., and Bales, R. C.: Higher surface mass balance of the Greenland ice sheet revealed by high-resolution climate modeling, Geophys. Res. Lett., 36, L12501, doi:10.1029/2009GL038110, 2009. 1051

Farrell, P. E., Ham, D. A., Funke, S. W., and Rognes, M. E.: Automated derivation of the adjoint of high-level transient finite element programs, arXiv:1204.5577, submitted, 2013. 1044

Fausto, R., Ahlstrom, A., As, D., Boggild, C., and Johnsen, S.: A new present-day temperature parameterization for Greenland, J. Glaciol., 55, 95–105, 2009. 1051

Favier, L., Gagliardini, O., Durand, G., and Zwinger, T.: A three-dimensional full Stokes model of the grounding line dynamics: effect of a pinning point beneath the ice shelf, The Cryosphere, 6, 101–112, doi:10.5194/tc-6-101-2012, 2012. 1055

Glen, J. W.: The creep of polycrystalline ice, P. Roy. Soc. Lond. A, 228, 519–538, 1955. 1035

Goldberg, D. N. and Sergienko, O. V.: Data assimilation using a hybrid ice flow model, The Cryosphere, 5, 315–327, doi:10.5194/tc-5-315-2011, 2011. 1033, 1043, 1044

Gottlieb, S. and Shu, C.: Total variation diminishing Runge–Kutta schemes, Math. Comput., 67, 73–85, 1998. 1045

Greve, R. and Hutter, K.: Polythermal three-dimensional modelling of the Greenland Ice Sheet with varied geothermal heat flux, Ann. Glaciol., 21, 8–12, 1995. 1032

Gudmundsson, G. H.: Transmission of basal variability to a glacier surface, J. Geophys. Res, 108, 2253, doi:10.1029/2002JB002107, 2003. 1054

Gudmundsson, G. H. and Raymond, M.: On the limit to resolution and information on basal properties obtainable from surface data on ice streams, The Cryosphere, 2, 167–178, doi:10.5194/tc-2-167-2008, 2008. 1033, 1043

Habashi, W. G., Dompierre, J., Bourgault, Y., Ait-Ali-Yahia, D., Fortin, M., and Vallet, M.-G.: Anisotropic mesh adaptation: towards user-independent, mesh-independent and solver-independent CF D. Part I: General principles, Int. J. Numer. Meth. Fl., 32, 725–744, doi:10.1002/(SICI)1097-0363(20000330)32:6<725::AID-FLD935>3.0.CO;2-4, 2000. 1042

Habermann, M., Maxwell, D., and Truffer, M.: Reconstruction of basal properties in ice sheets using iterative inverse methods, J. Glaciol., 58, 795–807, doi:10.3189/2012JoG11J168, 2012. 1044

Heroux, M. A., Bartlett, R. A., Howle, V. E., Hoekstra, R. J., Hu, J. J., Kolda, T. G., Lehoucq, R. B., Long, K. R., Pawlowski, R. P., Phipps, E. T., Salinger, A. G., Thornquist, H. K.,

TCD
7, 1029–1074, 2013

Tuminaro, R. S., Willenbring, J. M., Williams, A., and Stanley, K. S.: An overview of the Trilinos project, ACM T. Math. Software, 31, 397–423, doi:10.1145/1089014.1089021, 2005. 1040
Hutter, K.: A mathematical model of polythermal glaciers and ice sheets, Geophys. Astro. Fluid, 21, 201–224, doi:10.1080/03091928208209013, 1982. 1038
Johnson, J. V., Brinkerhoff, D. J., and Nowicki, S.: A novel mass onserving bed algorithm to estimate errors in bed elevation associated with flight line spacing, J. Geophys. Res., in review, 2013. 1033
Joughin, I., Smith, B. E., Howat, I. M., Scambos, T., and Moon, T.: Greenland flow variability from ice-sheet-wide velocity mapping, J. Glaciol., 56, 197, doi:10.3189/002214310792447734, 2010. 1051
Larour, E., Rignot, E., Joughin, I., and Aubry, D.: Rheology of the Ronne Ice Shelf, Antarctica, inferred from satellite radar interferometry data using an inverse control method, Geophys. Res. Lett., 32, L05503, doi:10.1029/2004GL021693, 2005. 1033, 1043
Larour, E., Seroussi, H., Morlighem, M., and Rignot, E.: Continental scale, high order, high spatial resolution ice sheet modeling using the Ice Sheet System Model (ISSM), J. Geophys. Res., 117, F01022, doi:10.1029/2011JF002140, 2012. 1031, 1032, 1033, 1044
Leng, W., Ju, L., Gunzburger, M., Price, S., and Ringler, T.: A parallel high-order accurate finite element nonlinear Stokes ice sheet model and benchmark experiments, J. Geophys. Res.-Earth, 117, F01001, doi:10.1029/2011JF001962, 2012. 1031, 1033
Logg, A., Mardal, K.-A., and Wells, G. N. (Eds.): Automated Solution of Differential Equations by the Finite Element Method, Springer, doi:10.1007/978-3-642-23099-8, 2012. 1040, 1048
MacAyeal, D. R.: A tutorial on the use of control methods in ice-sheet modeling, J. Glaciol., 39, 91–98, 1993. 1033, 1043
Morlighem, M., Rignot, E., Seroussi, H., Larour, E., Dhia, H. B., and Aubry, D.: Spatial patterns of basal drag inferred using control methods from a full-Stokes and simpler models for Pine Island Glacier, West Antarctica, Geophys. Res. Lett., 37, L14502, doi:10.1029/2010GL043853, 2010. 1033, 1043
Morlighem, M., Rignot, E., Seroussi, H., Larour, E., Dhia, H. B., and Aubry, D.: A mass conservation approach for mapping glacier ice thickness, Geophys. Res. Lett., 38, L19503, doi:10.1029/2011GL048659, 2011. 1033
Nocedal, J. and Wright, S.: Numerical Optimization, 2 Edn., Springer, USA, 2000. 1044
Nowicki, S. M. J.: Modelling the transition zone of marine ice sheets, Ph. D. thesis, University College London, 2007. 1055

TCD
7, 1029–1074, 2013

Pattyn, F.: A new three-dimensional higher-order thermomechanical ice-sheet model: basic sensitivity, ice-stream development and ice flow across subglacial lakes, J. Geophys. Res.-Sol. Ea., 108, 2382, doi:10.1029/2002JB002329, 2003. 1032, 1036, 1037, 1054

Pattyn, F., Perichon, L., Aschwanden, A., Breuer, B., de Smedt, B., Gagliardini, O., Gudmundsson, G. H., Hindmarsh, R. C. A., Hubbard, A., Johnson, J. V., Kleiner, T., Konovalov, Y., Martin, C., Payne, A. J., Pollard, D., Price, S., Rückamp, M., Saito, F., Souček, O., Sugiyama, S., and Zwinger, T.: Benchmark experiments for higher-order and full-Stokes ice sheet models (ISMIP-HOM), The Cryosphere, 2, 95–108, doi:10.5194/tc-2-95-2008, 2008. 1049

Payne, A. J., Huybrechts, P., Abe-Oughi, A., Calov, J. L. F. R., Greve, R., Marshall, S. J., Marsiat, I., Ritz, C., Tarasov, L., and Thomassen, M. P. A.: Results from the EISMINT model intercomparison: the effect of thermomechanical coupling, J. Glaciol., 46, 227–238, 2000. 1050

Pritchard, H. D., Arthern, R. J., Vaughan, D. G., and Edwards, L. A.: Extensive dynamic thinning on the margins of the Greenland and Antarctic ice sheets, Nature, 461, 971–975, doi:10.1038/nature08471, 2009. 1053

Rutt, I. C., Hagdorn, M., Hulton, N. R. J., and Payne, A. J.: The Glimmer community ice sheet model, J. Geophys. Res., 114, F02004, doi:10.1029/2008JF001015, 2009. 1031, 1032

Saito, F., Abe-Ouchi, A., and Blatter, H.: Effects of the first order stress gradients to an ice sheet evaluated by a three-dimensional thermo-mechanical coupled model, Ann. Glaciol., 37, 166–172, doi:10.3189/172756403781815645, 2003. 1054

Schoof, C.: Variational methods for glacier flow over plastic till, J. Fluid Mech., 555, 299–320, doi:10.1017/S0022112006009104, 2006. 1031

SeaRISE: SeaRISE website, http://websrv.cs.umt.edu/isis/index.php/SeaRISE_Assessment, 2012. 1051

Seddik, H., Greve, R., Zwinger, T., Gillet-Chaulet, F., and Gagliardini, O.: Simulations of the Greenland ice sheet 100 years into the future with the full Stokes model Elmer/Ice, J. Glaciol., 58, 427–440, 2012. 1031, 1032, 1033

Shapiro, N. M. and Ritzwoller, M. H.: Inferring surface heat distributions guided by global seismic model: particular applications to Antarctica, Earth Planet. Sci. Lett., 223, 69–84, 2004. 1051

Weis, M., Greve, R., and Hutter, K.: Theory of shallow ice shelves, Continuum Mech. Therm., 11, 15–50, 1999. 1043

TCD
7, 1029–1074, 2013

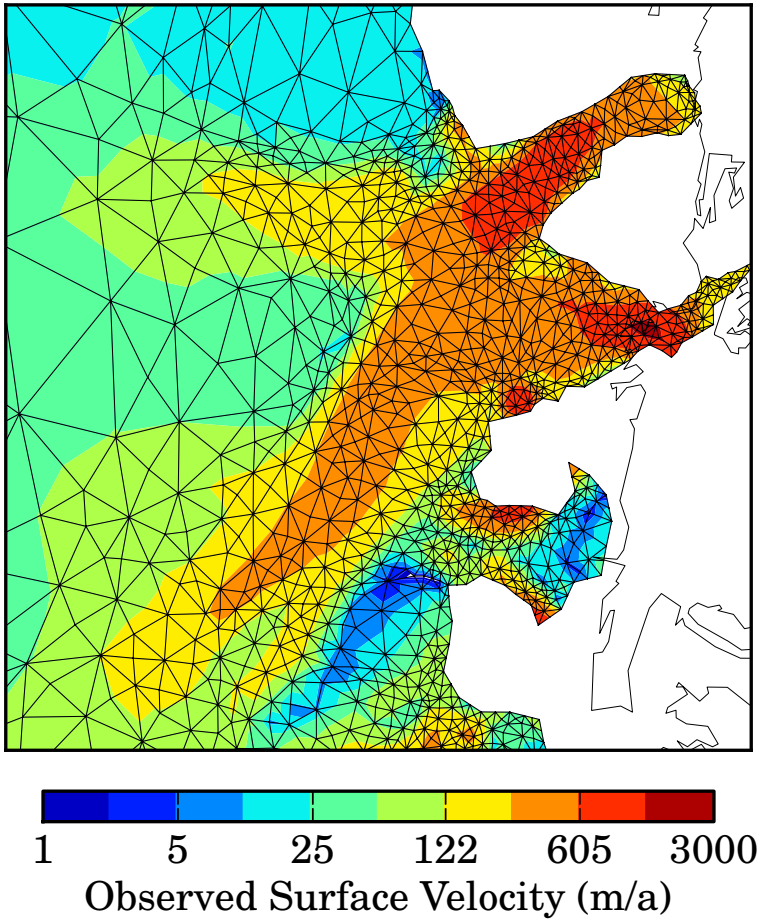

Fig. 1. Observed surface velocity projected onto an anisotropically refined mesh of Greenland's northeast ice stream.

TCD
7, 1029–1074, 2013

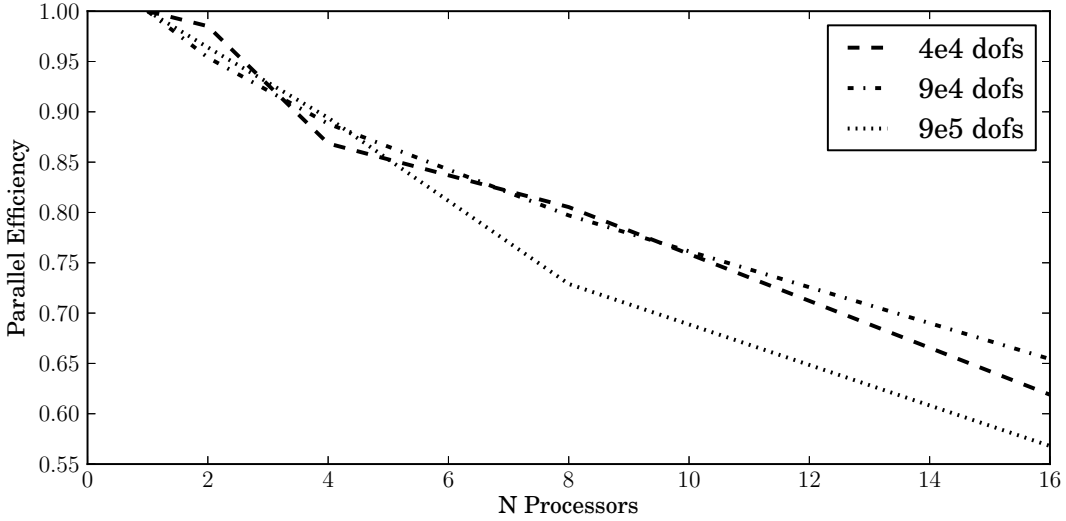

Fig. 2. Parallel efficiency computed for one complete Newton solve of the first order equations for meshes with different degrees of freedom. All linear solves were performed using parallel GMRES preconditioned with Hypre-AMG.

TCD
7, 1029–1074, 2013

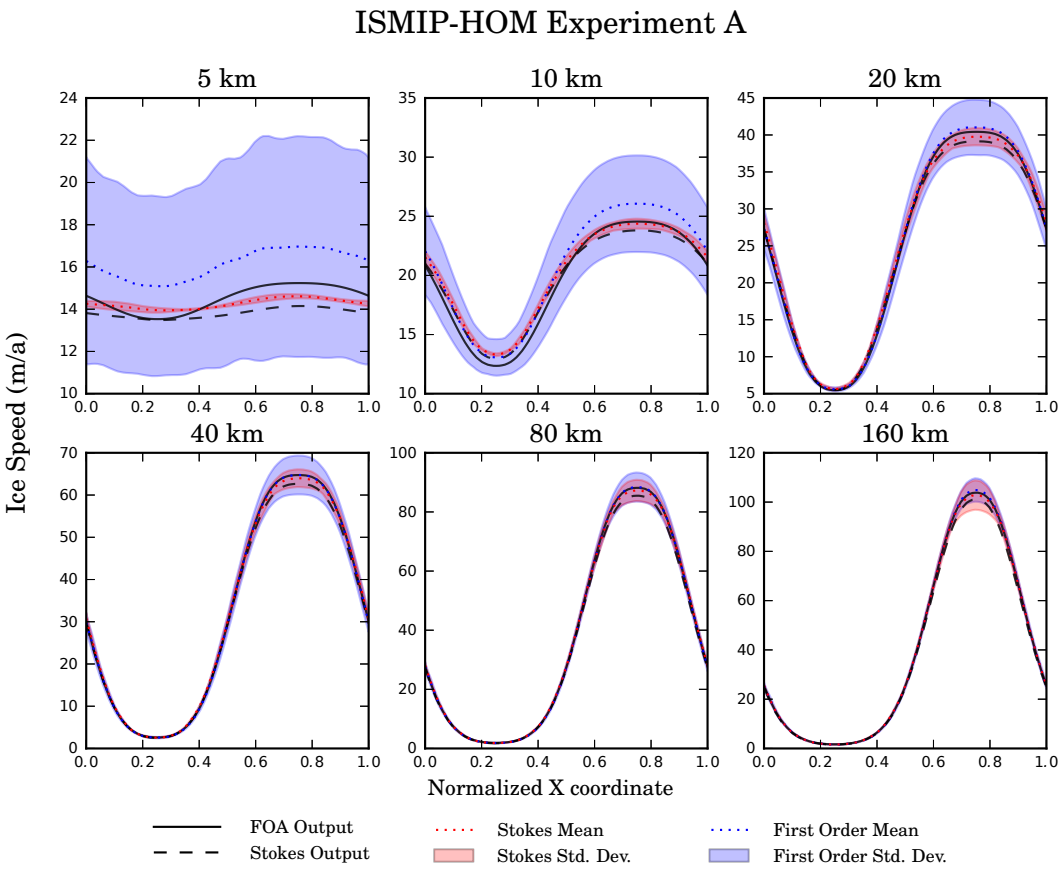

Fig. 3. ISMIP-HOM A performed using first order and Stokes' approximations.

TCD
7, 1029–1074, 2013

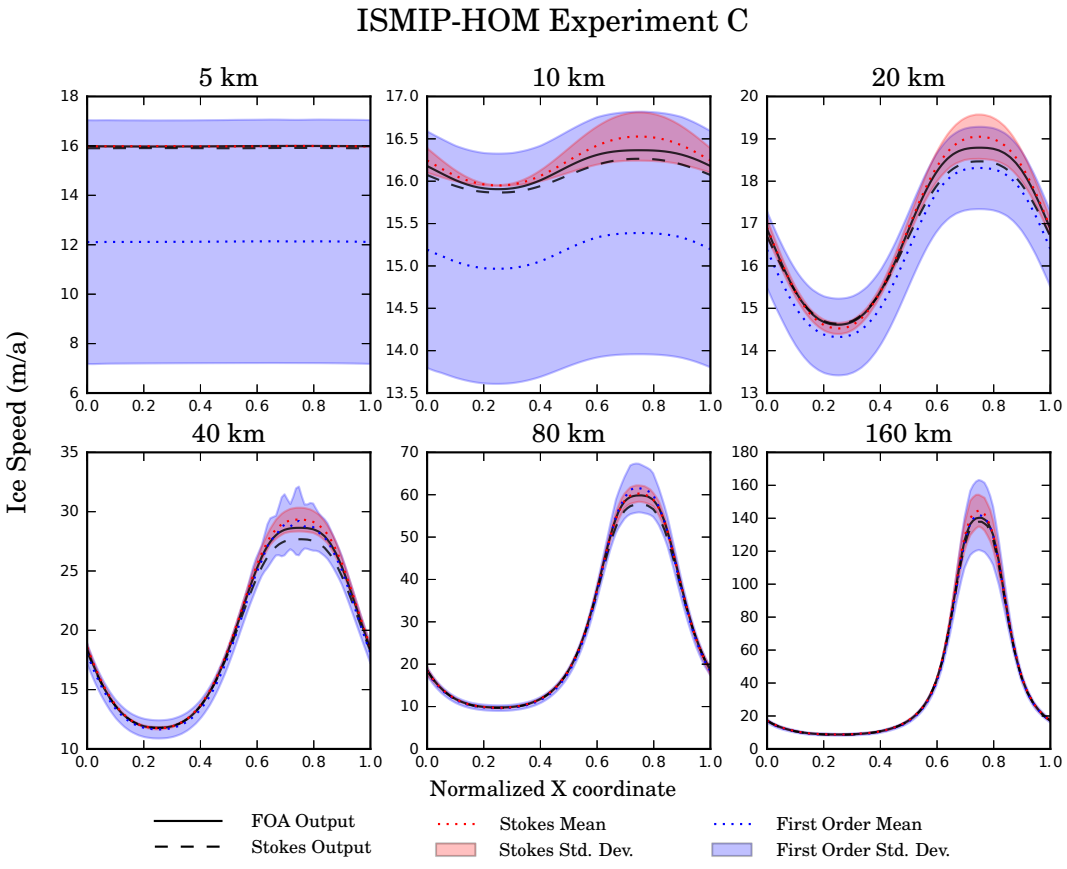

Fig. 4. ISMIP-HOM C performed using first order and Stokes' approximations.

TCD
7, 1029–1074, 2013

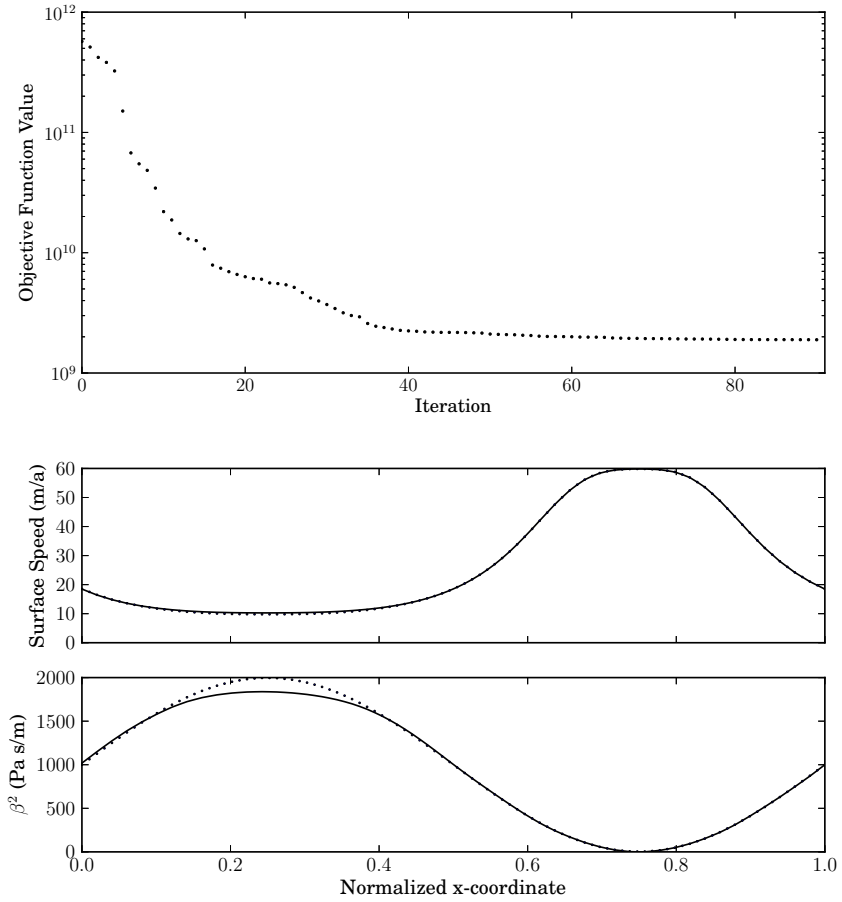

Fig. 5. Convergence profile and modelled basal traction and velocity from inverting ISMIP-HOM C.

TCD
7, 1029–1074, 2013

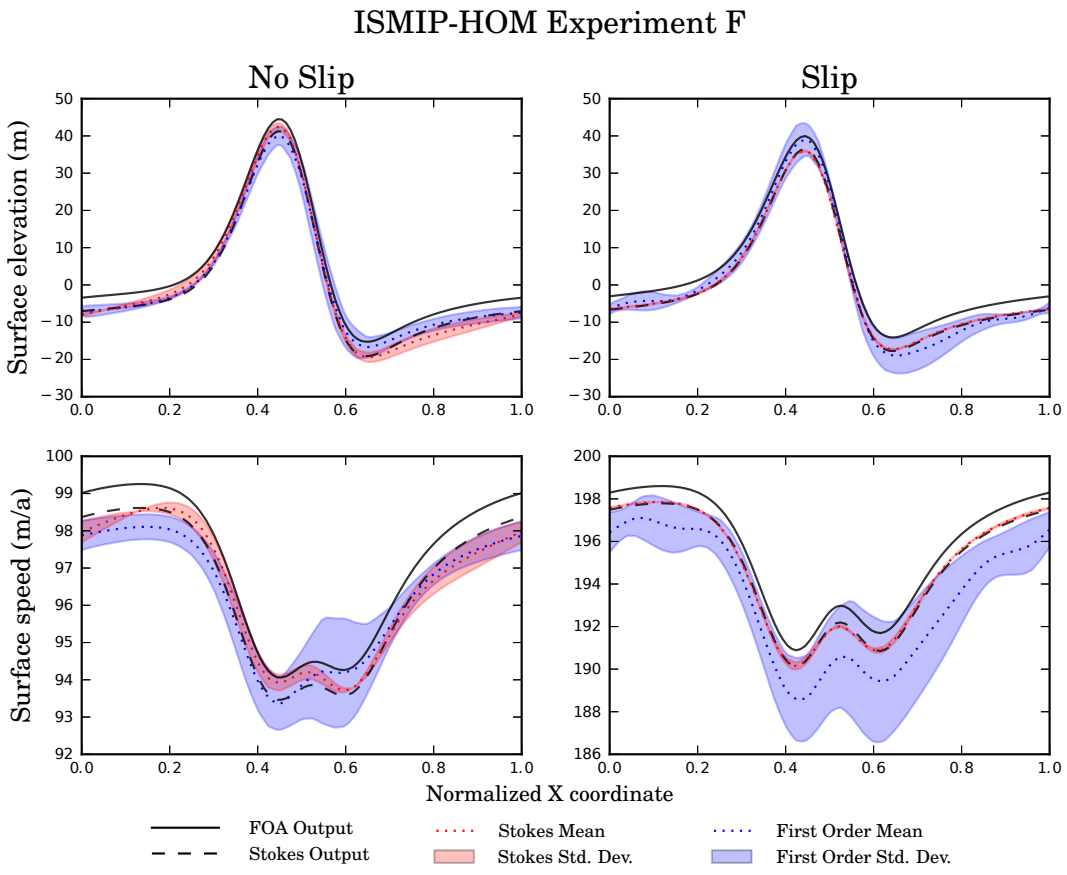

Fig. 6. ISMIP-HOM F performed using first order and Stokes' approximations.

TCD
7, 1029–1074, 2013

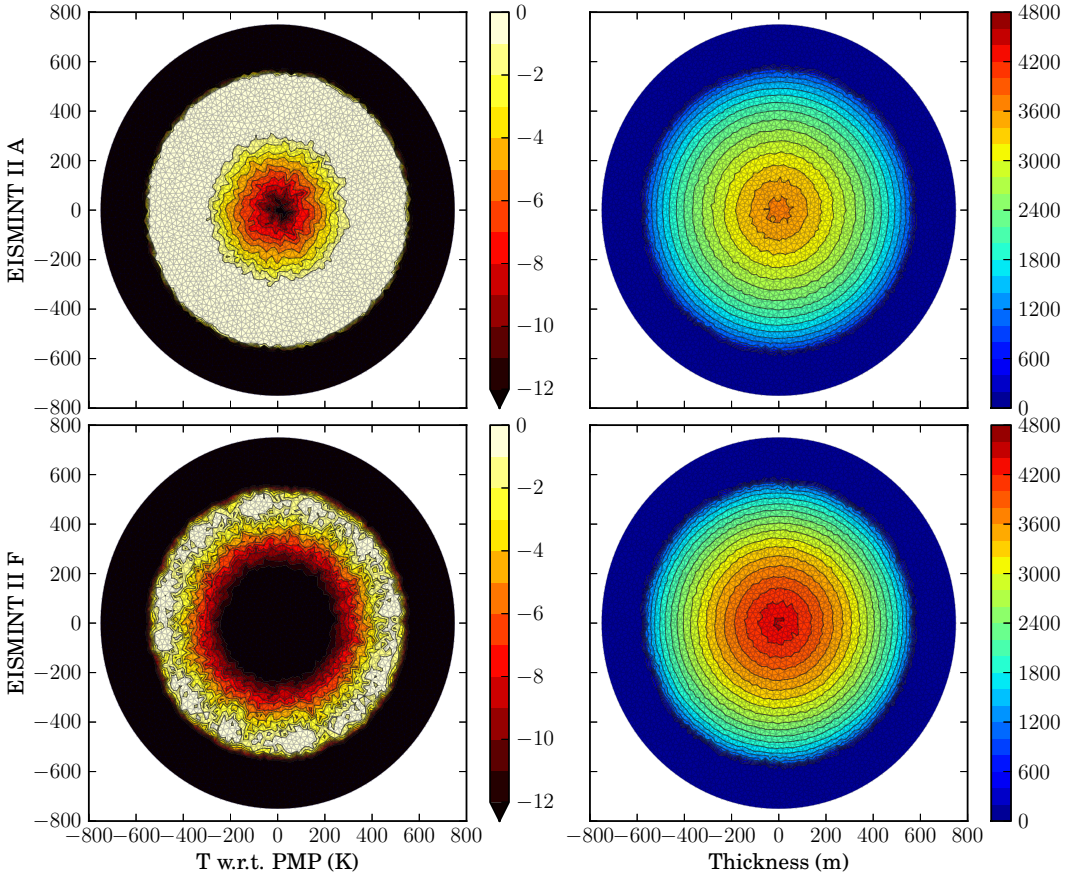

Fig. 7. Thickness and basal temperature fields for EISMINT II A and F at 200 ka.

TCD
7, 1029–1074, 2013

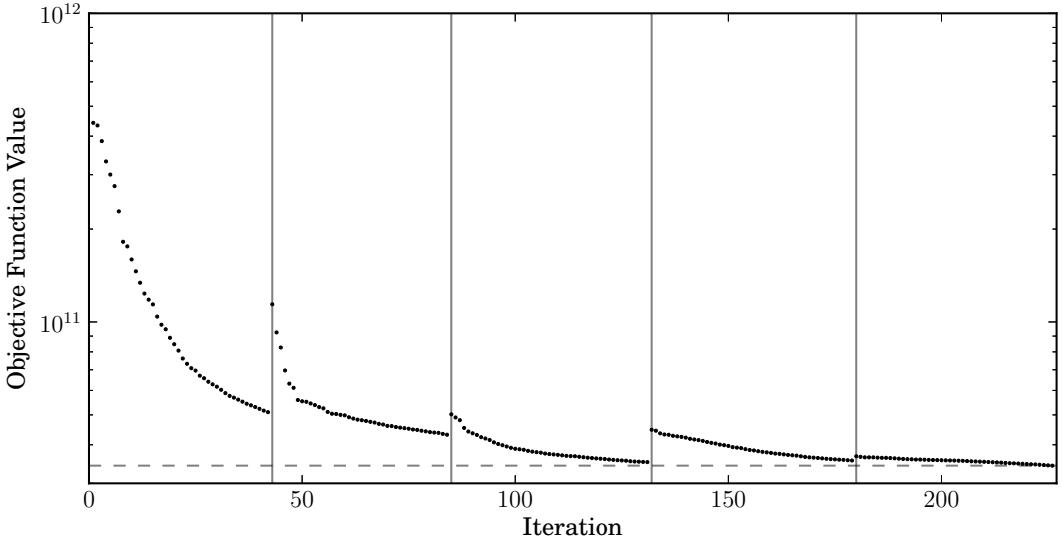

Fig. 8. Convergence rate of L_BFGS_B algorithm for surface velocity assimilation, using basal traction as a control variable. Vertical lines are where the enthalpy equations were recalculated.

TCD
7, 1029–1074, 2013

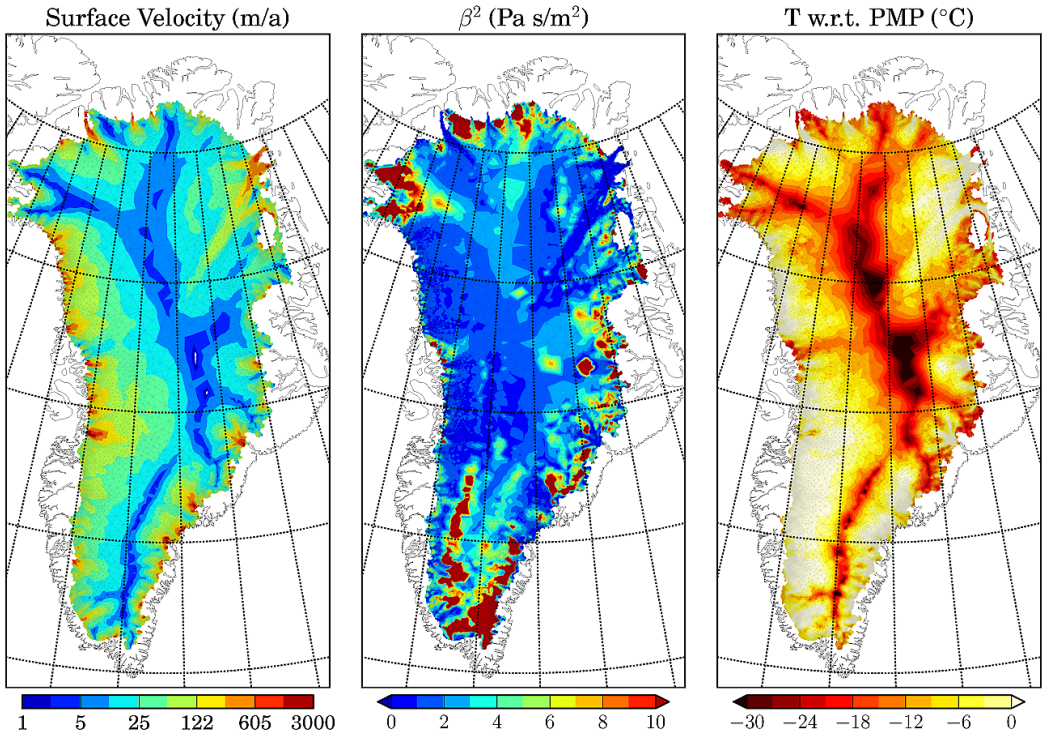

Fig. 9. Modelled surface velocity, basal traction, and basal temperature of the GIS after assimilation of surface velocity.

TCD
7, 1029–1074, 2013

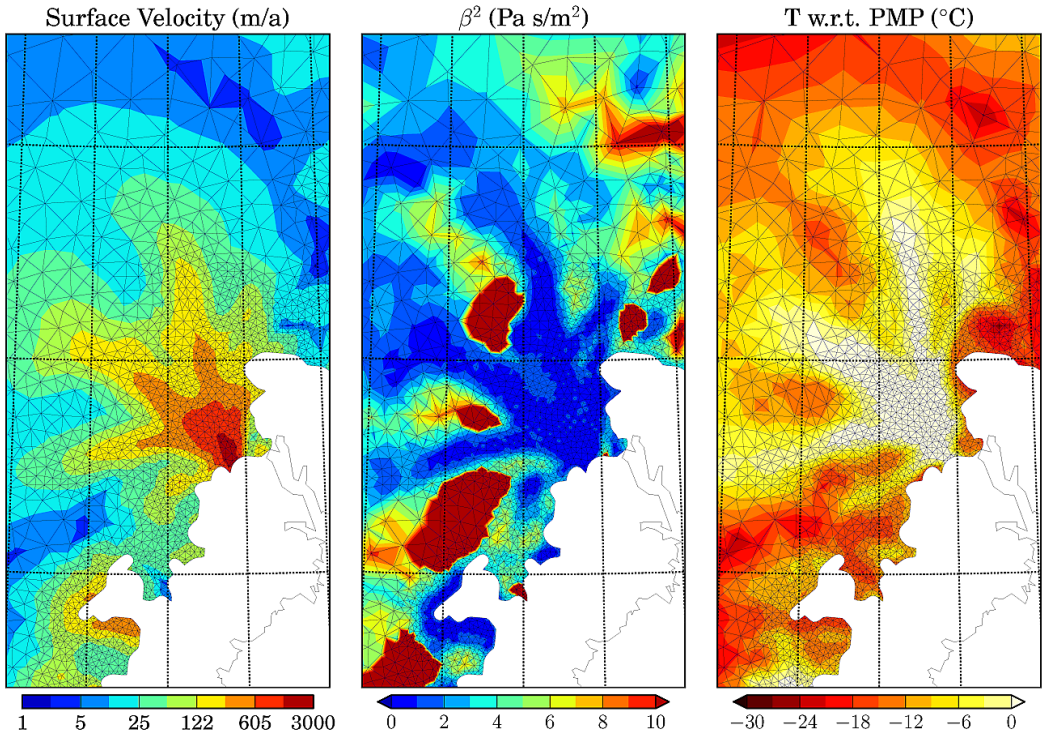

Fig. 10. Modelled surface velocity, basal traction, and basal temperature of Helheim glacier in eastern Greenland after assimilation of surface velocity.

TCD
7, 1029–1074, 2013

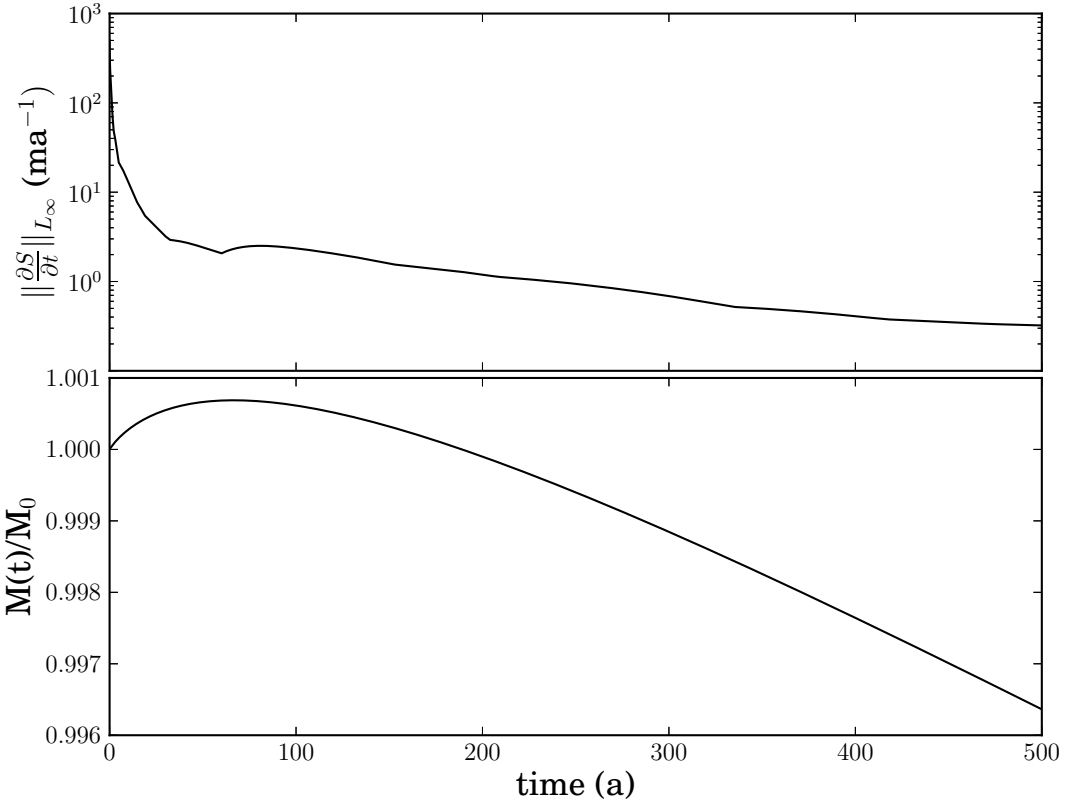

Fig. 11. The L_∞ norm of the surface elevation change field and the total ice mass over a 500 yr model run.

TCD
7, 1029–1074, 2013

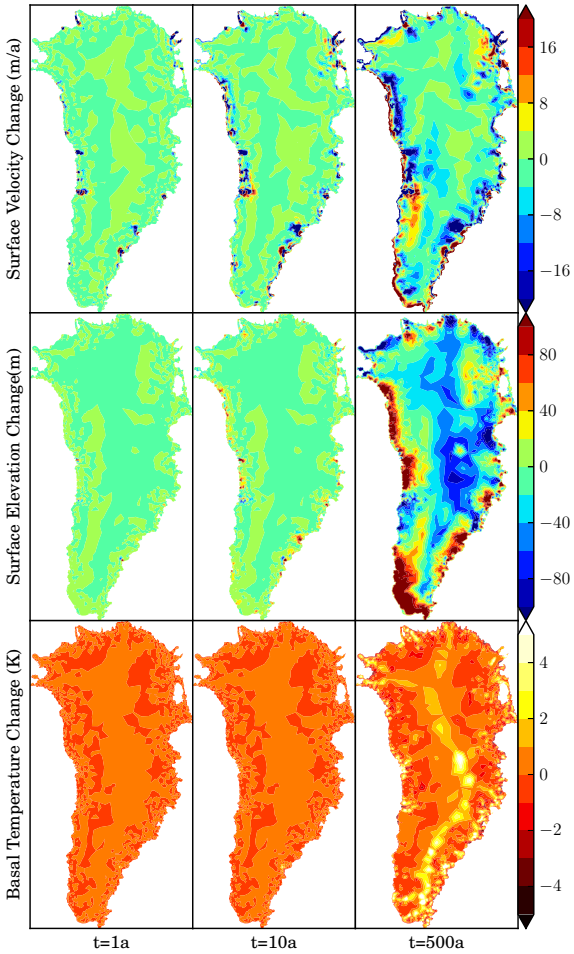

Fig. 12. Velocity, surface elevation, and basal temperature change through a 500 yr simulation of the Greenland Ice Sheet.

TCD
7, 1029–1074, 2013